



1 **Sea surface temperature evolution of the North Atlantic Ocean**
2 **across the Eocene-Oligocene Transition**

3 Kasia K. Śliwińska^{1,2,*}, Helen K. Coxall³, David K. Hutchinson^{3,4}, Diederik Liebrand⁵, Stefan Schouten^{2,6},
4 Agatha M. de Boer³

5 ¹Department of Stratigraphy, Geological Survey of Denmark and Greenland (GEUS), Øster Voldgade 10, 1350
6 Copenhagen, Denmark

7 ²NIOZ Royal Netherlands Institute for Sea Research, Department of Marine Microbiology and Biogeochemistry,
8 Landsdiep 4, 1797 SZ 't Horntje, Texel, the Netherland

9 ³Department of Geological Sciences, Stockholm University, Svante Arrhenius väg 8, 114 18 Stockholm, Sweden

10 ⁴Climate Change Research Centre, University of New South Wales, Sydney NSW 2052, Australia

11 ⁵National Oceanography Centre, European Way, SO14 3ZH, Southampton, United Kingdom

12 ⁶Department of Earth Sciences, Faculty of Geosciences, Utrecht University, Vening Meinesz building A, Princetonlaan
13 8a, 3584 CB Utrecht, the Netherlands

14

15 *Correspondence to:* Kasia K. Śliwińska (kksl@geus.dk)

16

17 **Key words:** sea surface temperature evolution, Eocene Oligocene Transition, Atlantic Ocean, coupled
18 climate model, ODP Site 647, southern Labrador Sea



Abstract. A major step in the long-term Cenozoic evolution toward a glacially-driven climate occurred at the Eocene Oligocene Transition (EOT), ~34.44 to 33.65 million years ago (Ma). Evidence for high latitude cooling and increased latitudinal temperature gradients across the EOT has been found in a range of marine and terrestrial environments. However, the timing and magnitude of temperature change in the North Atlantic remains highly unconstrained. Here, we use two independent organic geochemical paleo-thermometers to reconstruct sea surface temperatures (SSTs) from the southern Labrador Sea (Ocean Drilling Program - ODP Site 647) across the EOT. We find a permanent cooling step of ~3 °C (from 27 to 24 °C), between 34.9 Ma and 34.3 Ma, which is ~500 kyr prior to Antarctic glaciation. This step in SST values is asynchronous across Atlantic sites, signifying considerable spatiotemporal variability in SST evolution. However, it is part of an overall cooling observed across sites in the North Atlantic (NA) in the 5 million years bracketing the EOT. Such cooling is unexpected in light of proxy and modelling studies suggesting the startup or strengthening of the Atlantic Meridional Overturning Circulation (AMOC) before the EOT, which would warm the NA, although parallel Eocene CO₂ decline on the descent into the Oligocene icehouse might counter this feedback. Here we show, using a published modelling study, that a reduction in atmospheric CO₂ from 800 to 400 ppm is not sufficient to produce the observed cooling, if combined with NA warming from an AMOC startup, simulated here through Arctic closure from the Atlantic. Possible explanations of the apparent discrepancy are discussed and include uncertainty in the SST data, paleogeography and atmospheric CO₂ boundary conditions, model weaknesses, and an earlier AMOC startup that just strengthened at the EOT. The results highlight the remaining uncertainty in many aspects of data and modelling results which need to be improved before we can draw robust conclusions of the processes acting before and across the EOT.

1. Introduction

The principal signature of climatic change across the EOT in deep marine records is an apparent two-step positive increase in the oxygen isotopic ($\delta^{18}\text{O}$) composition of deep sea foraminifera, centered around 34 Ma (Zachos et al., 1996; Coxall et al., 2005) (Supplementary Information). Current understanding is that the first $\delta^{18}\text{O}$ step mostly reflects ocean cooling (Step 1; 33.9 Ma, known previously as EOT-1, see ref. (Hutchinson et al., 2021) and Table S01) and the second step reflects the accumulation of terrestrial ice on Antarctica (Lear et al., 2008; Bohaty et al., 2012; Zachos et al., 1996), which was recently redefined as the Early Oligocene oxygen Isotope Step (EOIS); at around 33.6 Ma, (Hutchinson et al., 2021), see also Supplementary Information). While a cooling signal is recorded in the benthic realm its absolute amplitude, expression at the surface ocean, and its global extent and uniformity remain largely unconstrained. A variety of data types support EOT cooling in the low latitudes and the Southern high latitudes, revealing temperature decreases that range between 2.5 to 5 °C in the deep sea (Bohaty et al., 2012; Lear et al., 2008; Pusz et al., 2011) and between 2 to 6 °C in surface waters and on land (Bohaty et al., 2012; Haiblen et al., 2019; Lauretano et al., 2021; Liu et al., 2009; Tibbett et al., 2021; Wade et al., 2012). Temperature evolution of the high northern latitudes, including regions of the North Atlantic Ocean where deep water is formed in the present day (Broecker, 1991; de Boer et al., 2008), however, remains less documented.

Existing low-resolution paleoclimate reconstructions from the Norwegian–Greenland Sea, including SST and terrestrial temperature constraints from palynology (Eldrett et al., 2009), organic molecular fossils (Liu et al., 2009; Schouten et al., 2008), and sediment grains (i.e., ice-rafted debris) (e.g. Eldrett et al., 2007), suggest some degree of cooling and increased seasonality concurrent with the EOT, which is possibly tied to relatively minor land-ice expansions on Greenland (Eldrett et al., 2007). Records from the mid-latitude North Atlantic report no SST change across the EOT as evidence of a temporary decoupling of the North Atlantic Ocean from the southern high latitudes and thus hemispherically asymmetric cooling, attributed to changes in circulation-driven heat transport (Liu et al., 2018). This existing suite of northern EOT temperature



60 records, still provide sparse coverage, with gaps at critical stages in the late Eocene and are of generally low temporal resolution. These data can therefore not be correlated in great detail to the EOT as identified in global benthic foraminiferal $\delta^{18}\text{O}$ records. This limits the understanding of cause-and-effect relationships with the much better resolved $\delta^{18}\text{O}$ and deep sea temperature records from the Southern Hemisphere (e.g. Hutchinson et al., 2021). A further stumbling block is that the quality of many northern North Atlantic records is often compromised by (i) carbonate dissolution in the sub-Arctic North Atlantic, limiting proxy based temperature estimates using foraminiferal calcite, and (ii) gaps in the sedimentary record at 65 many sites across the Eocene/Oligocene boundary that are caused by deep sea erosion (e.g. Miller et al., 1985).

Here we present newly generated proxy records of sea surface temperature from ODP Site 647 (53°20'N 45°16'W), located in the western North Atlantic, across an upper Eocene to middle Oligocene (i.e., time equivalent to 38–26.5 Ma) succession of hemipelagic clay from the southern Labrador Sea (Fig. 1). We use the TEX_{86} and $U_{37}^{K'}$ proxies, which are two independent 70 paleothermometers based on fossil organic biomarkers derived from archaea and photosynthetic plankton, respectively (Schouten et al., 2002; Brassell et al., 1986). These new data constitute the best-resolved EOT-spanning SST proxy records from the Northern hemisphere to date. They document patterns of temperature change in the north western Atlantic and help decipher the complex temperature evolution of the (North) Atlantic Ocean across the largest climate state-change of the Cenozoic Era.

75 We compare our newly obtained SST record to published SST proxy records and reconstruct latitudinal SST gradients for the Eocene and Oligocene in the North Atlantic. The compilation of SST records show cooling in the Atlantic across the EOT that one might expect as part of the global transitioning into an icehouse and which is usually attributed to a reduction in atmospheric CO_2 . (Anagnostou et al., 2016; Cramwinckel et al., 2018). Hypotheses for the CO_2 decrease abound and 80 include weathering or biological pump feedbacks from an AMOC startup (Hutchinson et al., 2021; Elsworth et al., 2017; Fyke et al., 2015). The AMOC has been suggested by multiple proxies to become active around the time of the EOT (Borrelli et al., 2021, 2014; Boyle et al., 2017; Coxall et al., 2018; Hutchinson et al., 2019; Kaminski and Ortiz, 2014, p.647; Langton et al., 2016; Uenzelmann-Neben and Gruetzner, 2018; Via and Thomas, 2006). Theory and modelling work have attributed the startup alternatively to Arctic Closure (Hutchinson et al., 2019), the deepening of Drake Passage and/or the 85 Tasman gateway (Toggweiler and Bjornsson, 2000), and the deepening of the Greenland Scotland Ridge (Stärz et al., 2017). However, a main feature of the AMOC is its northward heat transport in the Atlantic, which acts to make the NA warmer than it would otherwise be, begging the question of how AMOC warming and CO_2 cooling may combine to produce observed cooling in the NA. To address this question, we here analyze the SST in the modelling output from Hutchinson et al. (2018, 2019), in which they compared the impact of Arctic Closure and an atmospheric CO_2 decrease on the deep ocean circulaiton. They concluded that only the Arctic closure could lead to a startup of the AMOC at the EOT but here we focus 90 on the implications of these processes on SST.

The manuscript starts with a description of the drilling site and core, followed by detail on the various data methods used in the study and a description of the model and simulations. The results address first the specific SST time series in the Site 95 647 record and then puts it in the context of available NA SST records. The data are then compared to the modelling simulations and the implications for the processes in the NA and at the core site is discussed. We conclude with summary of the results and the potential implications for the state of knowledge of what happened at the EOT.



2. Labrador Sea Ocean Drilling Program Site 647

100 ODP Hole 647A constitutes the most northerly location (53°N) where a complete Eocene–Oligocene sedimentary sequence is known to be present (Coxall et al., 2018; Firth et al., 2013) (Fig. 1). The studied succession consists of grayish-green, moderately to strongly bioturbated nannofossil claystone and nannofossil chalk (see SI Lithostratigraphy of Site 647 for more information). The core recovery across the EOT (Cores 27R to 30R) is reasonable (Fig. S1). However, Core 29R is heavily disturbed and is usually omitted in the analysis of the site (Firth, 1989; Kaminski and Ortiz, 2014)). We have processed one sample from the Core 29R (29R-4, 130-132, 275.5 mbsf) for calcareous nannofossils and biomarkers. In the
105 sample we found neither caved (younger) nor reworked (older) calcareous nannofossil taxa (J. Firth personal communication 2013), thus, despite intra-core sediment mixing the analyzed biomarker signal remains stratigraphically useful, albeit producing a time-average SST signal, potentially for the whole Core C29. Also, even with some core disturbance and other minor core recovery gaps, a robust bio-magnetostratigraphic age model was obtained (Figs.2, 3, and S2). The datums included in the age model (following Firth et al., 2013) have been converted to the GTS2012 (Vandenberghe et al., 2012)
110 (Figs. 2,3, and S3). Additionally, the base of the chronozone C13n has here been tuned by comparison of the benthic foraminifera data from site 647A to the $\delta^{18}\text{O}$ record from Site 1218 (Coxall and Wilson, 2011). In the present study we use a low resolution Site 647 benthic $\delta^{18}\text{O}$ record for correlation purposes (Firth et al., 2013) (Fig. 2B). These $\delta^{18}\text{O}$ records can be directly correlated with the high resolution benthic reference curve from the eastern Equatorial Pacific (Site 1218) (Coxall and Wilson, 2011) used to identify $\delta^{18}\text{O}$ signatures of the Late Eocene, Step 1 and EOIS events in ODP Site 647A.

115 3. Methods

3.1. Biomarkers

Organic compounds were extracted from 71 sediment samples collected from the interval between 135.50 mbsf and 397.60 mbsf (15R 01W 10-20cm – 39R 02W 100-102cm). Samples were freeze-dried, mechanically powdered and 5-17g of sediment was taken for further analysis. The total lipid extract was obtained from sediments using the accelerated solvent
120 extraction (ASE) technique with dichloromethane (DCM):methanol (MeOH) (9:1, v/v). Excess solvent was removed by evaporation under Nitrogen in the TurboVap@LV for 1 hour under constant temperature (30°C) and constant gas pressure (15 psi). The total lipid extract was separated over an activated Al_2O_3 column into apolar (hexane:DCM, 1:1, v/v), ketone (hexane:DCM, 1:1 v/v) and polar (DCM:MeOH, 1:1, v/v) fractions, respectively.

3.1.1. Alkenone based temperature estimates

125 The ketone fraction was analysed for alkenones. Sufficient concentrations of di- and tri-unsaturated alkenones were detected in 32 uppermost samples (i.e. between 135.50 to 241.14 mbsf). In these samples we calculated sea surface temperatures by applying $U_{37}^{K'}$ proxy (Rodrigo-Gámiz et al., 2015).

First, the $U_{37}^{K'}$ index was calculated as follow:

$$U_{37}^{K'} = \frac{[37:2]}{[37:2]+[37:3]} \quad (1)$$

130 Second, the index was converted into temperature following the calibration of Müller et al., (1998).

$$T = U_{37}^{K'} - 0.044) / 0.033 \quad (2)$$



The T calibration error for Eq. (2) is $\pm 1.5^{\circ}\text{C}$. For seven samples, which were analyzed in duplicate, the reproducibility was better than 0.6°C (Fig. S2).

3.1.2. GDGT distribution

135 The polar fraction (containing glycerol dialkyl glycerol tetraethers; GDGTs) was concentrated under N_2 , dissolved in hexane/isopropanol (99:1, v/v), filtered using a $0.4\ \mu\text{m}$ PTFE filter and analyzed using high-pressure liquid chromatography (HPLC) as described by Schouten et al., (2007). Prior to calculating the sea surface temperatures from the TEX_{86} proxy, we have evaluated the source and the distribution of GDGTs.

140 For detecting a methanogenic input of GDGTs we applied the %GDGT-0 index (Sinninghe Damsté et al., 2012). Studies on enrichment cultures of Thaumarchaeota suggests that when %GDGT-0 values reach values above 67% the sedimentary GDGT pool may be affected by an additional (probably methanogenic) source of GDGTs. Our Eocene to Oligocene sediments show %GDGT-0 values between 26% and 63%, with a mean value of 41 % (Supplementary File) and thus the GDGT pool bears no signs of methanogenic source for the sedimentary archaea. Low values of the methane index (MI) (Zhang et al., 2011) and the GDGT-2/Crenarchaeol ratio (Weijers et al., 2011) (<0.25 and <0.13 , respectively) exclude input
145 of methanotrophic archaea versus Thaumarchaeota. The relative abundance of crenarchaeol isomer fCren':Cren' + Cren (O'Brien et al., 2017) in our dataset has values between 0.05 and 0.09 (Supplementary File) which is within the range (0.00-0.16) of values for the modern core-top sediments. In order to eliminate samples with GDGTs which may have been influenced by non-thermal factors we calculated the Ring Index (RI) (Zhang et al., 2016). Nine samples from our data set (12.5% of all samples, $n=71$) are excluded from the temperature calculations due to ΔRI above $|0.3|$ (Zhang et al., 2016)
150 (Supplementary File).

Fifteen samples (21% of all samples, $n=71$) were excluded from the temperature calculations because too high soil- and river-derived organic matter, as suggested by the BIT index (Hopmans et al., 2004). We used a cut-off value of 0.4 (Table S1). The BIT cut-off value for applicability of TEX_{86} as SST proxy depends on the particular location, i.e. the TEX_{86} value of the terrestrial GDGTs transported to the marine environment (see discussion in Schouten et al., 2013b) as well as the Mass
155 Spectrometer settings (Schouten et al., 2013a). In the studied interval the BIT index rarely exceeds 0.35 and shows no apparent trend in time. Furthermore, for the entire sample set, we find no correlation between BIT index and TEX_{86} ($R^2=0.01$).

3.1.3 TEX_{86}^H and BAYSPAR based temperature estimates

Due to BIT and/or ΔRI exceeding their cut-off values, 18 samples are excluded from the TEX_{86} compilation (see above). Out
160 of 71 sediment samples, 14 were analyzed in duplicate and two in triplicate. In our study we have applied two calibrations for TEX_{86} -derived SST estimations: the TEX_{86}^H linear calibration (Kim et al., 2010) and the TEX_{86} Bayesian regression model (BAYSPAR) (Tierney and Tingley, 2014, 2015). In the modern oceans the TEX_{86}^H is calculated as follows:

$$\text{TEX}_{86}^H = \log\left(\frac{[\text{GDGT-2}] + [\text{GDGT-3}] + [\text{Cren}']}{[\text{GDGT-1}] + [\text{GDGT-2}] + [\text{GDGT-3}] + [\text{Cren}']}\right) \quad (3)$$

Raw TEX_{86}^H values for the studied interval are between 0.56 and 0.71 with the mean value of 0.63 (1σ calibration
165 uncertainty). SST were subsequently calculated as follows:

$$\text{T } [^{\circ}\text{C}] = 68.4(\text{TEX}_{86}^H) + 38.6 \quad (4)$$

The T calibration error for Eq. (4) is $\sim 2.5^{\circ}\text{C}$. The analytical error of the SST derived from TEX_{86}^H is $\pm 0.6^{\circ}\text{C}$.



170 We also calculated SST predictions using the Bayesian regression model (BAYSPAR), for which we only included the sample set as for TEX_{86}^H . We computed SSTs using the online graphical user interface located at <http://bayspar.geo.arizona.edu> (accessed in 2017, currently discontinued) and inserted a paleolatitude of 45°N. Spatial analogues for deep-time for the BAYSPAR were calculated with the following settings:

- 1) Prior mean = 0.633639 (i.e. the mean TEX_{86} value for the timeseries)
- 2) Search tolerance = 0.072302 (i.e. 2*STDEV.P of timeseries)

175 The Bayesian estimates based on the TEX_{86} index values at Site 647A point to low latitude settings as modern analogues. TEX_{86}^H and BAYSPAR calibrations show very similar paleotemperature trends. The difference in SST is between 0°C and 0.6 °C for SST above 25.6°C, and between 0.8°C and 1.9°C for SST below 25.2 °C. Overall the mean difference in SST is 0.8°C. All the SST calibrations are shown in Fig. S2.

3.1.4. Potential bias of the TEX_{86} index

180 Some studies suggested that TEX_{86} reflect subsurface rather than surface temperatures (Lopes dos Santos et al., 2010; Huguet et al., 2007). However, $U_{37}^{K'}$ is a well-established proxy for SST and in our record TEX_{86} -derived temperatures are in close agreement with $U_{37}^{K'}$ -derived temperatures (Figs. 2, 3, and Fig. S2), suggesting that the temperatures recorded by GDGTs in our record can be used to indicate surface temperatures. Qin et al., (2015) questioned the application of the TEX_{86} proxy in sediments deposited under low O_2 concentrations. However, the nature of the benthic foraminiferal assemblages (e.g. Kaminski and Ortiz, 2014), signs of bioturbation throughout the recovered cores (Stein et al., 1989), and lack of other sedimentological features suggesting exceptionally low oxygen conditions (Srivastava and Arthur, 1987) across the interval covering the EOT, imply that the deposition took place under oxygenated waters (see also Kaminski and Ortiz, 2014). It has been also shown that oxic degradation of biomarker lipids can affect their relative distribution and thus the TEX_{86} (Huguet et al., 2009). However, we do not observe any signs of degradation in the analyzed material: such as a sharp increase in the BIT index values or a high degree of correlation between TEX_{86} and BIT.

3.2. Model simulations

The simulations were performed using the coupled climate model GFDL CM2.1 (Delworth et al., 2006) adapted to late Eocene (~38 Ma) boundary conditions, as outlined in Hutchinson et al., (2018). The model uses an ocean resolution of 1° x 1.5° x 50 levels and an atmosphere resolution of 3° x 3.75° x 24 levels. This allows better representation of ocean gateways than most existing Eocene-Oligocene climate models, which typically use ocean resolution of ~3°, or employ geographic boundary conditions not designed for this time interval. The model was run at two end-member CO_2 levels of 400 and 800 ppm, and spun up for 6500 years using an iterative coupling procedure, with the last 3200 years run in fully-coupled mode (Hutchinson et al., 2018). These experiments were carried out using modern day orbital forcing parameters. In the control configuration, the palaeogeography includes shallowly open ocean gateways between the Arctic and Norwegian-Greenland Sea as likely existed for some part of the late Eocene (Lasabuda et al., 2018; Straume et al., 2020). In this configuration, sinking occurs in the North Pacific and the Southern Ocean, but no deep water forms in the North Atlantic. We also simulated a modified version of the model with the Arctic-Atlantic gateway fully closed, as outlined in Hutchinson et al. (2019). This change dramatically increases the salinity in the North Atlantic and enables North Atlantic deep water to form. We thus compare the mean state and response to halving CO_2 from 800 to 400 ppm in a configuration where there is, and where there is not an AMOC present. All simulations were run for 6500 years, using the same spinup method as applied by



Hutchinson et al., (2018) except the the 400 ppm Arctic closed simulation which was branched from the 800 ppm Arctic closed configuration at year 5500 and continued for 1000 model years. This run is therefore further from equilibrium in the deep ocean than the corresponding 400 ppm run in the Arctic open configuration with shallowly open gateways.

4. Observations of SST

210 4.1. Sea surface temperatures in the Labrador Sea

Our Site 647 TEX_{86} -derived record shows high and relatively stable SSTs (~ 27 °C) in the southern Labrador Sea up to 35.5 Ma (Figs. 2, 3). Between ~ 35.5 and 34.9 Ma SSTs increased by ~ 1.5 °C. Subsequently, between ~ 34.9 Ma and ~ 34.3 Ma, SSTs decreased by ~ 3 – 4 °C, i.e. from 27 °C to 23–24 °C, depending on the TEX_{86} calibration (Fig. S1; the surface water cooling is reduced by ~ 1 °C when using TEX_{86}^H calibration). Between 34.3 Ma and 33 Ma, which includes the EOT interval, SSTs remained relatively stable (Fig. 2). Long chain alkenones, on which the U_{37}^{Kl} index is based, did not appear at Site 647 before ~ 33 Ma (Fig. 2). Once they appear, mean SST values derived from both U_{37}^{Kl} - and TEX_{86} are within the same range (Fig. S1) adding confidence in the absolute temperatures that we reconstruct. Both organic proxy temperature estimates are substantially higher than present day values (5–10 °C) (Fig. 2A), and in good accordance with available time-equivalent SST reconstructions for the region (Fig. 3).

220 Overall, we observe a permanent temperature decrease of ~ 3 – 4 °C at Site 647, when comparing the warmer Eocene with the colder Oligocene (Fig. 2, Tab. 1). Notably, most published SST data from the Atlantic Ocean (all shown in Fig. 3) are of (much) lower resolution and only bracket the main cooling and ice-growth events associated with the EOT. Our study provides the highest resolution, long term SST record from the North Atlantic region across the late Eocene, to date. It uniquely pinpoints the high northern latitude changes during the main climatic transitions and the critical lead-up period, by identifying a cooling in the southern Labrador Sea between 34.9 and 34.3 Ma, approximately 500 kyr prior to the Step 1 event (Fig 2A). This permanent temperature decrease falls within the range observed in the North Atlantic region, with a larger decrease across the EOT observed at Sites 336, 913 and Kysing-4 (North of Site 647), and a somewhat smaller SST decrease observed at Site U1404 (South of Site 647) (Fig. 3).

230 Remarkably, we find no change in SSTs at Site 647 concurrent with the Step 1 or EOIS events (Fig. 2), similar to the record from Site U1404 on the Newfoundland margin (Liu et al., 2018). The Labrador Sea surface cooling that predates the Step 1 event (Fig. 2) is also in agreement with a variety of other, more coarsely resolved northern hemisphere proxy reconstructions. These data include, e.g., dust records from Central Asia (Abels et al., 2011; Sun and Windley, 2015), which indicate that the strongest cooling and continental aridification occurred between 35 and 34 Ma, respectively. Lastly, this cooling (the Late Eocene event) is detected in several deep-sea records (e.g. ODP Site 689 in the Atlantic sector of the Southern Ocean) as a transient ~ 0.5 ‰ excursion in $\delta^{18}O$ and it probably coincides with a so-called ‘precursor glaciation’ on Antarctica (Hutchinson et al., 2021; Katz et al., 2008) interpreted to be driven by 405-kyr and ~ 110 -kyr eccentricity minima (Fig. S3). Based on these lines of evidence, we infer that the Late Eocene event had an impact on several globally distributed locations. However, the Atlantic sector of the Southern Ocean experienced only a transient cooling of bottom and surface waters of ~ 1 °C at that time (Bohaty et al., 2012), whereas our data suggests that during the Late Eocene event SSTs in the vicinity of Site 647 decreased more permanently.



4.2. Observed SST in the North Atlantic across the EOT

245 The still low resolution of SST data across the EOT in the NA, compared to time equivalent benthic $\delta^{18}\text{O}$ records, do not
allow for any detailed analysis of the changing spatial of temporal SST patterns in the NA, or identification of sequential
forcing mechanisms or leads of lags that could explain them. For example, in sites 336 and Kysing-4, where the data density
is high (~35.8 Ma), the SST data has a large range in a short interval, suggesting these are highly dynamic regions and more
so than site 647A (Fig. 3). In other sites like 913 there are only 6 data points between 32 Ma and 37 Ma, making it
250 impossible to identify temporal patterns or attribute them to internal or external variability. However, we combine the
available core data in an ensemble to derive an overarching picture of cooling across the 5 myrs bracketing the EOT in the NA.
Specifically, we calculate the average temperature values from 37.0 Ma to 34.5 Ma (“pre-34.5”) and from 34.5 Ma to 32.0
Ma (“post-34.5”) in all existing SST records in the North Atlantic region (Table S2). The threshold of 34.5 Ma is chosen,
because that is the where the clear shift towards colder temperatures in Site 647 is observed. We present the SST
255 temperatures in these two intervals as a function of latitude and note that the higher latitude cores are on average colder than
lower latitude cores, as one might expect (Fig. 4). The cooling across the EOT indicate polar amplification with stronger
cooling in the poleward sites such as 913 and 336 (Fig. 4), although we emphasize the high uncertainty in averaging so few
data points in these records.

5. Data-model comparison and implications

260 5.1 Absolute SST values before and after the SST

Here we compare the late Eocene “pre-34.5” and early Oligocene “post-34.5” SST at the five NA core sites to the four
combinations of an open and closed Arctic, and 400 and 800 ppm atmospheric CO_2 concentrations as described in
Hutchinson et al. (2018, 2019). Most of the simulations do a reasonable job at matching proxy SSTs at lower latitudes but
none of the simulations can produce the warm SSTs observed in the northern NA during the late Eocene (Fig. 4, 5),
265 suggesting that the model has too cold polar temperatures for the late Eocene. There may be several possible explanations for
this. The applied CO_2 concentration of 800 ppm may still be too low for the late Eocene. The existing $P_{\text{CO}_2^{\text{atm}}}$ reconstructions
across the EOT are of low resolution and are characterized by a large range of absolute values and relatively high levels of
uncertainty (Anagnostou et al., 2016; Steinthorsdottir et al., 2016; Zhang et al., 2013). However, it is unlikely that the
 $P_{\text{CO}_2^{\text{atm}}}$ was much more than 1000 ppm by the late Eocene (Fig 3a) so this is probably not the main reason for polar warmth
270 in the records compared to the model. Alternatively, it may be that the TEX_{86} -derived SST data is warmer than the model
output because it represents a summer signal. Several studies of TEX_{86} -derived SSTs of the Eocene greenhouse state suggest
the possibility of a summer bias at higher latitudes (e.g. Davies et al., 2019; Hollis et al., 2012). While some degree of
seasonal bias can not be ruled out, the overall trends and absolute SST estimates from the TEX_{86} proxy in our record
correspond well with those of $U_{37}^{K'}$ (Fig. S2). The $U_{37}^{K'}$ proxy is derived from haptophyte algae, which generally have different
275 bloom periods than Thaumarchaeota, and are thought to reflect annual mean or spring SST (Müller et al., 1998). This argues
at least against a strong seasonal bias in the $U_{37}^{K'}$ or TEX_{86} records. Alternatively, the model has too high polar temperatures
either because of too low climate sensitivity to CO_2 or insufficient polar amplification due to inadequate cloud feedbacks
(Baatsen et al., 2020; Lunt et al., 2021). The simulation with the higher 800 ppm CO_2 and the closed Arctic (with active
AMOC) gives the warmest absolute temperature in the NA and is therefore the closest to observations both for the late
280 Eocene and early Oligocene (pink dashed line in Fig. 4, Fig. 5d).



5.2 SST change across the EOT in the NA

As detailed above, the EOT cooling is usually attributed to a decrease in atmospheric CO₂ and numerous studies have suggested that an accelerated CO₂ decrease may have been triggered by the startup of the AMOC at or just prior to the EOT. The open and closed Arctic simulations shown here are part of one such study in which the NA deep water formation is activated through closing off of the freshwater pathways from the Arctic to the Atlantic (Hutchinson, 2019). The AMOC is known to transport heat northward in the Atlantic and its collapse in the modern climate is associated with cooler NA SSTs (Jackson et al., 2015). We see the same at the EOT, with a startup of the AMOC through closing the Arctic causing a >5 °C temperature increase in the subpolar gyre (Fig. 6a,b). The warming from the AMOC startup is greater in the colder 400 ppm climate than the warmer 800 ppm climate, probably because of a stronger meridional temperature gradient in the cooler climate that produces more northward heat transport. The cooling from a reduction in atmospheric CO₂ is of similar magnitude as the AMOC warming, albeit slightly weaker and with a different spatial pattern (Fig. 6c,d). This greenhouse cooling is stronger when the connection to the Arctic is open and the AMOC is off. Not only is the meridional overturning circulation weaker in this case but also the horizontal circulation in both the Subtropical and Subpolar gyres (Fig. 7). If may be the that stronger meridional heat transport in the Arctic closed case reduced the polar amplification of the cooling.

To investigate whether greenhouse cooling could compensate for AMOC warming at the EOT we compare the 800 ppm Arctic open simulation with the 400 ppm Arctic closed simulation (Fig. 6e). While there is an overall cooling in the Arctic and Subtropical gyre, there remains a warming signal in the Subpolar gyre, which is inconsistent with the cooling trend across the EOT from the data. Unfortunately at the higher Subpolar latitudes, where temperature anomalies in both simulations and observations are largest, the data is also the most sparse. Nevertheless, the lack of cooling in northern NA temperature, if we combine greenhouse cooling and an AMOC startup, requires explanation. The first possibility is that the AMOC did not start up at or just prior to the EOT but started earlier and just intensified 500 kyr prior to the EOT (Coxall et al., 2018). The change in heat transport from a strengthening should be less than from a complete cold start up. Alternatively, the Arctic gateways changes could have been more subtle in reality than in the model, thus dampening the impact on the circulation and SST, or the AMOC may have started up through an altogether different mechanism such as the widening of the Southern Gateways (Elsworth et al., 2017) which could have a smaller warming effect. This process of starting up the AMOC did not work in the modeling study of Hutchinson et al. (2019) but such results can be model dependent and requires corroboration. There are also model deficiencies that could explain the overall NA warming, such as the above mentioned exaggerated meridional temperature gradient in the model at the EOT (causing too much heat transport through the AMOC) and too low climate sensitivity to the CO₂ decrease. Another point to mention is that the model produces deep water in the Labrador Sea and Greenland Sea when the Arctic is closed-off (Hutchinson et al., 2019), yet there is no evidence in Site 647 records for deep water formation in the Labrador Sea before or directly after the EOT (Cramwinckel et al., 2020; Coxall et al., 2018). The model AMOC is therefore feeding deep water from two regions instead of one and thus likely too strong. Finally, the CO₂ cooling could be greater if there was a larger drop in CO₂ across the EOT. However, while it is reasonable that the pre-EOT CO₂ was higher than 800 ppm, there is little evidence that it may have been as low as 400 ppm after the EOT (Fig 3a).

5.3 Local SST variability at site 647.

With its higher temporal resolution compared to other NA records at the time, it is interesting to note some temporal signals in the SST at Site 647 across the late Eocene. In particular, there is a minimum in temperature at ~35.7 Ma and a maximum at ~34.9 Ma after which the permanent cooling of the EOT occurs (Fig 3). The SST at Site 647 seems reasonably stable, in



that its data points that are close together in time have similar SSTs, unlike for instance at Site 336 and Kysing-4 where temperature oscillates by 5°C within 200 kyrs at ~35.6 Ma (Fig 3). The variability described here at Site 647 is well resolved and does not rely on individual data points, except arguably for the minimum at 35.7 Ma. The increase in SST between 35.7 Ma and 34.9 Ma could possibly be due to an increase in the AMOC at the time which culminated at 34.9 Ma (Coxall et al., 2018). Thereafter, normal background CO₂ cooling could have resumed. A peak in SST was also observed during this time at low latitude Atlantic Site 959 (Cramwinckle et al., 2018). Other Atlantic sites have too low resolution records to study this type of variability so this point remains speculative. Today Site 647 is located in the south-western part of the North Atlantic Subpolar gyre, influenced by cold and low-salinity subarctic surface waters. The model suggests that at the EOT the site was in or near the warmer Subtropical gyre and switched from the Subtropical to the Subpolar gyres in the scenario where the Arctic closed and CO₂ dropped from 800 to 400 ppm (Fig. 7). The position and strength of the gyres are likely model dependent and should not be taken too literally, but suffice to say that it depends critically on the paleogeography in the region which was dynamic at the time (Hutchinson et al., 2019). A simple shift of the gyre boundary could suddenly mean the site is bathed in polar water or subtropical waters and this could be a result of a number of drivers such as the paleogeography or the CO₂. All these drivers affect the NA at large and in particular the northern latitudes. Even a globally homogenous forcing factor such as CO₂ concentrations result through regional feedback in inhomogenous changes in the NA SST (Fig 6).

6. Conclusions

Our new SST record derived from organic geochemical paleo-thermometers provide the highest resolution of SST across the EOT in the Northern NA to date. We detect SST variability in the 2.5 myr leading up to the EOT, which includes a ~ 800 kyr warming interval before the final cooling step 500 kyr before the EOT. Model simulations of various possible paleogeographic and atmospheric CO₂ scenarios at the time, indicate that the site is located in a dynamic region close to the Subtropical and Subpolar gyre boundary and SST variability could suggest a movement of the gyre boundary across the site area. Such a movement could be driven by global atmospheric CO₂ or local or global paleogeographic changes. Whatever the driver, our model suggest that there is usually some coherence in the NA SST response across the Subpolar gyre and separately the Subtropical gyre, but in general the response is heterogeneous across the NA. Any extrapolation of ocean warming or cooling at a specific site location to the wider Atlantic and global climate drivers should therefore be done with care.

In order to compare the SST changes across the EOT with other NA lower resolution records, the SST was averaged over a late Eocene bin spanning the 2.5 Myr before the 34.9 cooling step in core 647, and the early Oligocene bin spanning the 2.5 Myrs after this step. In this basin wide view, the cooling at the EOT is found to be larger at higher latitudes, although this is also where data is particularly sparse. The binned data was compared to four model simulations of EOT scenarios with high and low atmospheric CO₂ and open and closed Arctic-Atlantic gateways, also representing off and on AMOC scenarios, respectively. The cooling across the EOT is best simulated with a drop in CO₂ alone. If the AMOC started up at or just prior to the EOT, then according to our model, despite the background greenhouse cooling, it would have caused an overall warming in the Subpolar NA which is not observed. It is possible that the AMOC did not start up in the late Eocene, but an alternative explanation is then required for the deep ocean circulation proxies at the (Coxall et al., 2018). Also, if the EOT cooling was driven by stand alone CO₂ changes, the question remains, why was there a sharp deep ocean cooling step before Antarctic ice-sheet growth (Lear et al., 2008). Other possibilities are (i) that the AMOC started up earlier and just intensified at the EOT, (ii) that the model is over estimating the AMOC heat transport due to too warm polar temperature at the Eocene,



(iii) that the CO₂ decrease is larger than modelled here, or (iv) that the model has too low sensitivity to CO₂ cooling. It should be noted that the model time slices present only a few possible scenarios of which none were probably an exact reality at any point. The pre- and post-EOT world would not correspond to any single scenario but would be a dynamic time of variable paleo-geography and CO₂.

365

Our new data aids in understanding of the timing and the spatial pattern of temperature changes related to the transition into the unipolar icehouse climate state. The model simulations highlight the heterogeneity of NA SST and its response to different forcing factors. This calls for more SST data, and greater understanding of the ocean-climate signal they carry, to fully understand the evolution of the surface water currents in the North Atlantic-Arctic region across this major climatic transition in conjunction with more model simulations to establish the robustness of the SST and deep ocean response to various climate drivers.

370

Acknowledgments

This research was funded by the Danish Council for Independent Research/Natural Sciences (DFF/FNU; grant 11-107497) to K.K.Ś., Swedish Research Council (VR) grants awarded to A.M.dB (2016-03912 and 2020-04791) and H.K.C. (2008-2859), Formas grant to D.K.H. (2018-01621) and the Netherlands Earth System Science Centre (NESSC) and the Ministry of Education, Culture and Science (OCW) to S.S.. The model simulations were enabled by resources provided by the Swedish National Infrastructure for Computing (SNIC) at the National Supercomputer Centre (NSC), partially funded by the Swedish Research Council through grant agreement no. 2016-07213. We thank Walter Hale at Bremen Core Repository (BCR) for collecting samples. We appreciate inspiring discussions with J. Firth and J. Backman and laboratory assistance from A. Metz. This research used samples provided by the Ocean Drilling Project (ODP). ODP was sponsored by the U.S. National Science Foundation and participating countries under management of Joint Oceanographic Institutions.

380

Availability of data

The new data are available in the Supplementary Information files. The model data used in this analysis will be made available upon publication in an open access database hosted by the Bolin Centre for Climate Research (<https://bolin.su.se/data/>).

385

Authorship contribution statement

K.K.Ś. designed the research. K.K.Ś and S.S. generated organic geochemical proxy (TEX₈₆, U^K₃₇) data. H.K.C helped to produce the Site 647 age model and correlate with IODP Site 1218. D.K.H. ran all model simulations. K.K.Ś and AMdB were the main authors of the manuscript, although all authors contributed with data interpretation and writing.

390

Author information

The authors declare no competing financial interests. Correspondence should be addressed to K.K.Ś. (kksl@geus.dk)

395

References

Abels, H. A., Dupont-Nivet, G., Xiao, G., Bosboom, R., and Krijgsman, W.: Step-wise change of Asian interior climate preceding the Eocene-Oligocene Transition (EOT), <https://doi.org/10.1016/j.palaeo.2010.11.028>, 2011.

400

Anagnostou, E., John, E. H., Edgar, K. M., Foster, G. L., Ridgwell, A., Inglis, G. N., Pancost, R. D., Lunt, D. J., and Pearson, P. N.: Changing atmospheric CO₂ concentration was the primary driver of early Cenozoic climate, 533, 380–384, <https://doi.org/10.1038/nature17423>, 2016.



- 405 Arthur, M. A., Srivastava, S. P., Kaminski, M., Jarrard, R., and Osler, J.: Seismic Stratigraphy and History of Deep Circulation and Sediment Drift Development in Baffin Bay and the Labrador Sea, in: Proceedings of the Ocean Drilling Program, 105 Scientific Results, 957–988, <https://doi.org/10.2973/odp.proc.sr.105.118.1989>, 1989.
- 410 Baatsen, M., von der Heydt, A. S., Huber, M., Kliphuis, M. A., Bijl, P. K., Sluijs, A., and Dijkstra, H. A.: The middle to late Eocene greenhouse climate modelled using the CESM 1.0.5, 16, 2573–2597, <https://doi.org/10.5194/cp-16-2573-2020>, 2020.
- de Boer, A. M., Toggweiler, J. R., and Sigman, D. M.: Atlantic Dominance of the Meridional Overturning Circulation, <https://doi.org/10.1175/2007JPO3731.1>, 2008.
- Bohaty, S. M., Zachos, J. C., and Delaney, M. L.: Foraminiferal Mg/Ca evidence for Southern Ocean cooling across the Eocene-Oligocene transition, 317–318, 251–261, <https://doi.org/10.1016/j.epsl.2011.11.037>, 2012.
- 415 Borrelli, C., Cramer, B. S., and Katz, M. E.: Bipolar Atlantic deepwater circulation in the middle-late Eocene: Effects of Southern Ocean gateway openings, <https://doi.org/10.1002/2012PA002444>, 2014.
- Borrelli, C., Katz, M. E., and Toggweiler, J. R.: Middle to Late Eocene Changes of the Ocean Carbonate Cycle, 36, e2020PA004168, <https://doi.org/10.1029/2020PA004168>, 2021.
- 420 Boyer, T. P., Antonov, J. I., Baranova, O. K., Garcia, H. E., Johnson, D. R., Mishonov, A. V., O'Brien, T. D., Seidov, D., I. (Igor), S., Zweng, M. M., Paver, C. R., Locarnini, R. A., Reagan, J. R., Coleman, C., and Grodsky, A.: World ocean database 2013, NOAA Atlas NESDIS 72, <https://doi.org/10.7289/V5NZ85MT>, 2013.
- Boyle, P. R., Romans, B. W., Tucholke, B. E., Norris, R. D., Swift, S. A., and Sexton, P. F.: Cenozoic North Atlantic deep circulation history recorded in contourite drifts, offshore Newfoundland, Canada, <https://doi.org/10.1016/j.margeo.2016.12.014>, 2017.
- 425 Brassell, S. C., Eglinton, G., Marlowe, I. T., Pflaumann, U., and Sarnthein, M.: Molecular stratigraphy: A new tool for climatic assessment, <https://doi.org/10.1038/320129a0>, 1986.
- Broecker, W.: The Great Ocean Conveyor, <https://doi.org/10.5670/oceanog.1991.07>, 1991.
- Coxall, H. K. and Wilson, P. A.: Early Oligocene glaciation and productivity in the eastern equatorial Pacific: Insights into global carbon cycling, 26, <https://doi.org/10.1029/2010PA002021>, 2011.
- 430 Coxall, H. K., Wilson, P. A., Pälike, H., Lear, C. H., and Backman, J.: Rapid stepwise onset of Antarctic glaciation and deeper calcite compensation in the Pacific Ocean, 433, 53–57, <https://doi.org/10.1038/nature03135>, 2005.
- 435 Coxall, H. K., Huck, C. E., Huber, M., Lear, C. H., Legarda-Lisarrí, A., O'Regan, M., Śliwińska, K. K., van de Flierdt, T., de Boer, A. M., Zachos, J. C., and Backman, J.: Export of nutrient rich Northern Component Water preceded early Oligocene Antarctic glaciation, 11, 190–196, <https://doi.org/10.1038/s41561-018-0069-9>, 2018.
- Cramwinckel, M. J., Huber, M., Kocken, I. J., Agnini, C., Bijl, P. K., Bohaty, S. M., Frieling, J., Goldner, A., Hilgen, F. J., Kip, E. L., Peterse, F., van der Ploeg, R., Röhl, U., Schouten, S., and Sluijs, A.: Synchronous tropical and polar temperature evolution in the Eocene, 559, 382–386, <https://doi.org/10.1038/s41586-018-0272-2>, 2018.
- 440 Cramwinckel, M. J., Coxall, H. K., Śliwińska, K. K., Polling, M., Harper, D. T., Bijl, P. K., Brinkhuis, H., Eldrett, J. S., Houben, A. J. P., Peterse, F., Schouten, S., Reichert, G.-J., Zachos, J. C., and Sluijs, A.: A Warm, Stratified, and Restricted Labrador Sea Across the Middle Eocene and Its Climatic Optimum, 35, e2020PA003932, <https://doi.org/10.1029/2020PA003932>, 2020.
- 445 Davies, A., Hunter, S. J., Gréselle, B., Haywood, A. M., and Robson, C.: Evidence for seasonality in early Eocene high latitude sea-surface temperatures, *Earth and Planetary Science Letters*, 519, 274–283, <https://doi.org/10.1016/j.epsl.2019.05.025>, 2019.



- Davies, R., Cartwright, J., Pike, J., and Line, C.: Early Oligocene initiation of North Atlantic Deep Water formation., 410, 917–920, <https://doi.org/10.1038/35073551>, 2001.
- 450 Delworth, T. L., Broccoli, A. J., Rosati, A., Stouffer, R. J., Balaji, V., Beesley, J. A., Cooke, W. F., Dixon, K. W., Dunne, J., Dunne, K. A., Durachta, J. W., Findell, K. L., Ginoux, P., Gnanadesikan, A., Gordon, C. T., Griffies, S. M., Gudgel, R., Harrison, M. J., Held, I. M., Hemler, R. S., Horowitz, L. W., Klein, S. A., Knutson, T. R., Kushner, P. J., Langenhorst, A. R., Lee, H.-C., Lin, S.-J., Lu, J., Malyshev, S. L., Milly, P. C. D., Ramaswamy, V., Russell, J., Schwarzkopf, M. D., Shevliakova, E., Sirutis, J. J., Spelman, M. J., Stern, W. F., Winton, M., Wittenberg, A. T., Wyman, B., Zeng, F., and Zhang, R.: GFDL's CM2 Global Coupled Climate Models. Part I: Formulation and Simulation Characteristics, 19, 643–674, <https://doi.org/10.1175/JCLI3629.1>, 2006.
- 455 Eldrett, J. S., Harding, I. C., Wilson, P. A., Butler, E., and Roberts, A. P.: Continental ice in Greenland during the Eocene and Oligocene, 446, 176–179, <https://doi.org/10.1038/nature05591>, 2007.
- Eldrett, J. S., Greenwood, D. R., Harding, I. C., and Huber, M.: Increased seasonality through the Eocene to Oligocene transition in northern high latitudes, 459, 969–973, <https://doi.org/10.1038/nature08069>, 2009.
- 460 Elsworth, G., Galbraith, E., Halverson, G., and Yang, S.: Enhanced weathering and CO₂ drawdown caused by latest Eocene strengthening of the Atlantic meridional overturning circulation, 10, 213–216, 2017.
- Firth, J. V.: Eocene and Oligocene calcareous nannofossils from the Labrador Sea, ODP Leg 105, 105, 263–286, 1989.
- 465 Firth, J. V., Eldrett, J. S., Harding, I. C., Coxall, H. K., and Wade, B. S.: Integrated biomagnetostratigraphy for the Palaeogene of ODP Hole 647A: implications for correlating palaeoceanographic events from high to low latitudes, 373, 29–78, <https://doi.org/10.1144/SP373.9>, 2013.
- Fyke, J. G., D'Orgeville, M., and Weaver, A. J.: Drake Passage and Central American Seaway controls on the distribution of the oceanic carbon reservoir, 128, 72–82, <https://doi.org/10.1016/j.gloplacha.2015.02.011>, 2015.
- 470 Haiblen, A. M., Opdyke, B. N., Roberts, A. P., Heslop, D., and Wilson, P. A.: Midlatitude Southern Hemisphere Temperature Change at the End of the Eocene Greenhouse Shortly Before Dawn of the Oligocene Icehouse, 34, 1995–2004, <https://doi.org/10.1029/2019PA003679>, 2019.
- Hohbein, M. W., Sexton, P. F., and Cartwright, J. A.: Onset of North Atlantic deep water production coincident with inception of the Cenozoic global cooling trend, 40, 255–258, <https://doi.org/10.1130/G32461.1>, 2012.
- 475 Hollis, C. J., Taylor, K. W. R., Handley, L., Pancost, R. D., Huber, M., Creech, J. B., Hines, B. R., Crouch, E. M., Morgans, H. E. G., Crampton, J. S., Gibbs, S., Pearson, P. N., and Zachos, J. C.: Early Paleogene temperature history of the Southwest Pacific Ocean: Reconciling proxies and models, 349–350, 53–66, <https://doi.org/10.1016/j.epsl.2012.06.024>, 2012.
- Hopmans, E. C., Weijers, J. W. H., Schefuß, E., Herfort, L., Sinninghe Damsté, J. S., and Schouten, S.: A novel proxy for terrestrial organic matter in sediments based on branched and isoprenoid tetraether lipids, 224, 107–116, <https://doi.org/10.1016/j.epsl.2004.05.012>, 2004.
- 480 Houben, A. J. P., Quaijtaal, W., Wade, B. S., Schouten, S., and Brinkhuis, H.: Quantitative organic-walled dinoflagellate cyst stratigraphy across the Eocene-Oligocene Transition in the Gulf of Mexico: A record of climate- and sea level change during the onset of Antarctic glaciation, nos, 52, 131–154, <https://doi.org/10.1127/nos/2018/0455>, 2019.
- 485 Huguet, C., Schimmelmann, A., Thunell, R., Lourens, L. J., Sinninghe Damsté, J. S., and Schouten, S.: A study of the TEX₈₆ paleothermometer in the water column and sediments of the Santa Barbara Basin, California, 22, 1–9, <https://doi.org/10.1029/2006PA001310>, 2007.
- 490 Huguet, C., Kim, J. H., de Lange, G. J., Sinninghe Damsté, J. S., and Schouten, S.: Effects of long term oxic degradation on the U37 K', TEX₈₆ and BIT organic proxies, <https://doi.org/10.1016/j.orggeochem.2009.09.003>, 2009.



- Hutchinson, D. K., De Boer, A. M., Coxall, H. K., Caballero, R., Nilsson, J., and Baatsen, M.: Climate sensitivity and meridional overturning circulation in the late Eocene using GFDL CM2.1, 14, 789–810, <https://doi.org/10.5194/cp-14-789-2018>, 2018.
- 495 Hutchinson, D. K., Coxall, H. K., O'Regan, M., Nilsson, J., Caballero, R., and de Boer, A. M.: Arctic closure as a trigger for Atlantic overturning at the Eocene-Oligocene Transition, *Nat Commun*, 10, 3797, <https://doi.org/10.1038/s41467-019-11828-z>, 2019.
- Hutchinson, D. K., Coxall, H. K., Lunt, D. J., Steinthorsdottir, M., de Boer, A. M., Baatsen, M., von der Heydt, A., Huber, M., Kennedy-Asser, A. T., Kunzmann, L., Ladant, J.-B., Lear, C. H., Moraweck, K., Pearson, P. N., Piga, E., Pound, M. J., Salzmann, U., Scher, H. D., Sijp, W. P., Śliwińska, K. K., Wilson, P. A., and Zhang, Z.: The Eocene–Oligocene transition: a review of marine and terrestrial proxy data, models and model–data comparisons, *Clim. Past*, 17, 269–315, <https://doi.org/10.5194/cp-17-269-2021>, 2021.
- 500 Inglis, G. N., Farnsworth, A., Lunt, D., Foster, G. L., Hollis, C. J., Pagani, M., Jardine, P. E., Pearson, P. N., Markwick, P., Galsworthy, A. M. J., Raynham, L., Taylor, K. W. R., and Pancost, R. D.: Descent toward the Icehouse: Eocene sea surface cooling inferred from GDGT distributions, 30, 1000–1020, <https://doi.org/10.1002/2014PA002723>, 2015.
- 505 Jackson, L. C., Kahana, R., Graham, T., Ringer, M. A., Woollings, T., Mecking, J. V., and Wood, R. A.: Global and European climate impacts of a slowdown of the AMOC in a high resolution GCM, *Clim Dyn*, 45, 3299–3316, <https://doi.org/10.1007/s00382-015-2540-2>, 2015.
- Kaminski, M. A. and Ortiz, S.: The Eocene–Oligocene turnover of deep-water agglutinated foraminifera at ODP Site 647, Southern Labrador Sea (North Atlantic), 60, 53–66, 2014.
- 510 Kaminski, M. A., Gradstein, F. M., and Berggren, W. A.: Paleogene benthic foraminifer biostratigraphy and paleoecology at Site 647, southern Labrador Sea, 105, 705–730, 1989.
- Katz, M. E., Miller, K. G., Wright, J. D., Wade, B. S., Browning, J. V., Cramer, B. S., and Rosenthal, Y.: Stepwise transition from the Eocene greenhouse to the Oligocene icehouse, 1, 329–334, <https://doi.org/10.1038/ngeo179>, 2008.
- 515 Kim, J. H., van der Meer, J., Schouten, S., Helmke, P., Willmott, V., Sangiorgi, F., Koç, N., Hopmans, E. C., and Damsté, J. S. S.: New indices and calibrations derived from the distribution of crenarchaeal isoprenoid tetraether lipids: Implications for past sea surface temperature reconstructions, 74, 4639–4654, <https://doi.org/10.1016/j.gca.2010.05.027>, 2010.
- 520 Langton, S. J., Rabideaux, N. M., Borrelli, C., and Katz, M. E.: Southeastern Atlantic deep-water evolution during the late-middle Eocene to earliest Oligocene (Ocean Drilling Program Site 1263 and Deep Sea Drilling Project Site 366), 12, 1032–1047, 2016.
- Lasabuda, A., Laberg, J. S., Knutsen, S.-M., and Høgseth, G.: Early to middle Cenozoic paleoenvironment and erosion estimates of the southwestern Barents Sea: Insights from a regional mass-balance approach, *Marine and Petroleum Geology*, 96, 501–521, <https://doi.org/10.1016/j.marpetgeo.2018.05.039>, 2018.
- 525 Lauretano, V., Kennedy-Asser, A. T., Korasidis, V. A., Wallace, M. W., Valdes, P. J., Lunt, D. J., Pancost, R. D., and Naafs, B. D. A.: Eocene to Oligocene terrestrial Southern Hemisphere cooling caused by declining pCO₂, *Nat. Geosci.*, 14, 659–664, <https://doi.org/10.1038/s41561-021-00788-z>, 2021.
- Lear, C. H., Bailey, T. R., Pearson, P. N., Coxall, H. K., and Rosenthal, Y.: Cooling and ice growth across the Eocene-Oligocene transition, 36, 251–254, <https://doi.org/10.1130/G24584A.1>, 2008.
- 530 Liu, Z., Pagani, M., Zinniker, D., DeConto, R., Huber, M., Brinkhuis, H., Shah, S. R., Leckie, R. M., and Pearson, A.: Global cooling during the Eocene-Oligocene climate transition, 323, 1187–1190, <https://doi.org/10.1126/science.1166368>, 2009.



- 535 Liu, Z., He, Y., Jiang, Y., Wang, H., Liu, W., Bohaty, S. M., and Wilson, P. A.: Transient temperature asymmetry between hemispheres in the Palaeogene Atlantic Ocean, *Nature Geoscience*, <https://doi.org/10.1038/s41561-018-0182-9>, 2018.
- 540 Lopes dos Santos, R. A., Prange, M., Castañeda, I. S., Schefuß, E., Mulitza, S., Schulz, M., Niedermeyer, E. M., Sinninghe Damsté, J. S., and Schouten, S.: Glacial-interglacial variability in Atlantic meridional overturning circulation and thermocline adjustments in the tropical North Atlantic, *300*, 407–414, <https://doi.org/10.1016/j.epsl.2010.10.030>, 2010.
- 545 Lunt, D. J., Bragg, F., Chan, W.-L., Hutchinson, D. K., Ladant, J.-B., Morozova, P., Niezgodzki, I., Steinig, S., Zhang, Z., Zhu, J., Abe-Ouchi, A., Anagnostou, E., de Boer, A. M., Coxall, H. K., Donnadieu, Y., Foster, G., Inglis, G. N., Knorr, G., Langebroek, P. M., Lear, C. H., Lohmann, G., Poulsen, C. J., Sepulchre, P., Tierney, J. E., Valdes, P. J., Volodin, E. M., Dunkley Jones, T., Hollis, C. J., Huber, M., and Otto-Bliesner, B. L.: DeepMIP: model intercomparison of early Eocene climatic optimum (EECO) large-scale climate features and comparison with proxy data, *17*, 203–227, <https://doi.org/10.5194/cp-17-203-2021>, 2021.
- Miller, K. G., Mountain, G. S., and Tucholke, B. E.: Oligocene glacio-eustasy and erosion on the margins of the North Atlantic., [https://doi.org/10.1130/0091-7613\(1985\)13<10:OGAEOT>2.0.CO;2](https://doi.org/10.1130/0091-7613(1985)13<10:OGAEOT>2.0.CO;2), 1985.
- 550 Müller, P. J., Kirst, G., Ruhland, G., Von Storch, I., and Rosell-Melé, A.: Calibration of the alkenone paleotemperature index U37Kbased on core-tops from the eastern South Atlantic and the global ocean (60°N–60°S), [https://doi.org/10.1016/S0016-7037\(98\)00097-0](https://doi.org/10.1016/S0016-7037(98)00097-0), 1998.
- 555 O'Brien, C. L., Robinson, S. A., Pancost, R. D., Sinninghe Damsté, J. S., Schouten, S., Lunt, D. J., Alsenz, H., Bornemann, A., Bottini, C., Brassell, S. C., Farnsworth, A., Forster, A., Huber, B. T., Inglis, G. N., Jenkyns, H. C., Linnert, C., Littler, K., Markwick, P., McAnena, A., Mutterlose, J., Naafs, B. D. A., Püttmann, W., Sluijs, A., van Helmond, N. A. G. M., Vellekoop, J., Wagner, T., and Wrobel, N. E.: Cretaceous sea-surface temperature evolution: Constraints from TEX86 and planktonic foraminiferal oxygen isotopes, <https://doi.org/10.1016/j.earscirev.2017.07.012>, 2017.
- 560 Ortiz, S. and Kaminski, M. A.: Record of Deep-Sea, Benthic Elongate-Cylindrical Foraminifera Across the Eocene-Oligocene Transition in the North Atlantic Ocean (ODP Hole 647A), *42*, 345–368, <https://doi.org/10.2113/gsjfr.42.4.345>, 2012.
- Pagani, M., Huber, M., Liu, Z., Bohaty, S. M., Henderiks, J., Sijp, W., Krishnan, S., and DeConto, R. M.: The role of carbon dioxide during the onset of antarctic glaciation, *334*, 1261–1264, <https://doi.org/10.1126/science.1203909>, 2011.
- 565 Pearson, P. N., Foster, G. L., and Wade, B. S.: Atmospheric carbon dioxide through the Eocene–Oligocene climate transition, *461*, 1110–1113, 2009.
- Piepjohn, K., von Gosen, W., and Tessensohn, F.: The Eurekan deformation in the Arctic: an outline, *jgs2016-081*, <https://doi.org/10.1144/jgs2016-081>, 2016.
- Pusz, A. E., Thunell, R. C., and Miller, K. G.: Deep water temperature, carbonate ion, and ice volume changes across the Eocene-Oligocene climate transition, *26*, PA2205, <https://doi.org/10.1029/2010PA001950>, 2011.
- 570 Qin, W., Carlson, L. T., Armbrust, E. V., Devol, A. H., Moffett, J. W., Stahl, D. A., and Ingalls, A. E.: Confounding effects of oxygen and temperature on the TEX₈₆ signature of marine Thaumarchaeota., *112*, 10979–10984, <https://doi.org/doi:10.1073/pnas.1501568112>, 2015.
- 575 Rodrigo-Gámiz, M., Rampen, S. W., de Haas, H., Baas, M., Schouten, S., and Sinninghe Damsté, J. S.: Constraints on the applicability of the organic temperature proxies UK'37, TEX86 and LDI in the subpolar region around Iceland, *12*, 6573–6590, <https://doi.org/10.5194/bg-12-6573-2015>, 2015.
- Schouten, S., Hopmans, E. C., Schefuß, E., and Sinninghe Damsté, J. S.: Distributional variations in marine crenarchaeol membrane lipids: a new tool for reconstructing ancient sea water temperatures?, [https://doi.org/10.1016/S0012-821X\(03\)00193-6](https://doi.org/10.1016/S0012-821X(03)00193-6), 2002.



- 580 Schouten, S., Hugué, C., Hopmans, E. C., Kienhuis, M. V. M., and Damsté, J. S. S.: Analytical methodology for TEX₈₆ paleothermometry by high-performance liquid chromatography/atmospheric pressure chemical ionization-mass spectrometry, <https://doi.org/10.1021/ac062339v>, 2007.
- Schouten, S., Eldrett, J., Greenwood, D. R., Harding, I., Baas, M., and Damsté, J. S. S.: Onset of long-term cooling of Greenland near the Eocene-Oligocene boundary as revealed by branched tetraether lipids, 36, 147–150, <https://doi.org/10.1130/G24332A.1>, 2008.
- 585 Schouten, S., Hopmans, E. C., Rosell-Melé, A., Pearson, A., Adam, P., Bauersachs, T., Bard, E., Bernasconi, S. M., Bianchi, T. S., Brocks, J. J., Carlson, L. T., Castañeda, I. S., Derenne, S., Selver, A. D., Dutta, K., Eglinton, T., Fosse, C., Galy, V., Grice, K., Hinrichs, K. U., Huang, Y., Hugué, A., Hugué, C., Hurley, S., Ingalls, A., Jia, G., Keely, B., Knappy, C., Kondo, M., Krishnan, S., Lincoln, S., Lipp, J., Mangelsdorf, K., Martínez-García, A., Ménot, G., Mets, A., Mollenhauer, G., Ohkouchi, N., Ossebaar, J., Pagani, M., Pancost, R. D., Pearson, E. J.,
- 590 Peterse, F., Reichert, G. J., Schaeffer, P., Schmitt, G., Schwark, L., Shah, S. R., Smith, R. W., Smittenberg, R. H., Summons, R. E., Takano, Y., Talbot, H. M., Taylor, K. W. R., Tarozo, R., Uchida, M., Van Dongen, B. E., Van Mooy, B. A. S., Wang, J., Warren, C., Weijers, J. W. H., Werne, J. P., Woltering, M., Xie, S., Yamamoto, M., Yang, H., Zhang, C. L., Zhang, Y., Zhao, M., and Damsté, J. S. S.: An interlaboratory study of TEX₈₆ and BIT analysis of sediments, extracts, and standard mixtures, 14, 5263–5285, <https://doi.org/10.1002/2013GC004904>,
- 595 2013a.
- Schouten, S., Hopmans, E. C., and Sinninghe Damsté, J. S.: The organic geochemistry of glycerol dialkyl glycerol tetraether lipids: A review, <https://doi.org/10.1016/j.orggeochem.2012.09.006>, 2013b.
- Sinninghe Damsté, J. S., Ossebaar, J., Schouten, S., and Verschuren, D.: Distribution of tetraether lipids in the 25-ka sedimentary record of Lake Challa: extracting reliable TEX₈₆ and MBT/CBT palaeotemperatures from an equatorial African lake, 50, 43–54, <https://doi.org/10.1016/J.QUASCIREV.2012.07.001>, 2012.
- Śliwińska, K. K., Thomsen, E., Schouten, S., Schoon, P. L., and Heilmann-Clausen, C.: Climate- and gateway-driven cooling of Late Eocene to earliest Oligocene sea surface temperatures in the North Sea Basin, *Sci Rep*, 9, 4458, <https://doi.org/10.1038/s41598-019-41013-7>, 2019.
- Srivastava, S. P. and Arthur, M. A.: Site 647 (ODP), 1987.
- 605 Stein, R., Littke, R., Stax, R., and Welte, D.: Quantity, provenance, and maturity of organic matter at ODP Sites 645, 646, and 647: implications for reconstruction of paleoenvironments in Baffin Bay and Labrador Sea during Tertiary and Quaternary time, 105, 185–208, 1989.
- Steinthorsdóttir, M., Porter, A. S., Holohan, A., Kunzmann, L., Collinson, M., and McElwain, J. C.: Fossil plant stomata indicate decreasing atmospheric CO₂ prior to the Eocene-Oligocene boundary, 12, 439–454, <https://doi.org/10.5194/cp-12-439-2016>, 2016.
- 610 Straume, E. O., Gaina, C., Medvedev, S., and Nisancioglu, K. H.: Global Cenozoic Paleobathymetry with a focus on the Northern Hemisphere Oceanic Gateways, *Gondwana Research*, 86, 126–143, <https://doi.org/10.1016/j.gr.2020.05.011>, 2020.
- Sun, J. and Windley, B. F.: Onset of aridification by 34 Ma across the Eocene-Oligocene transition in Central Asia, <https://doi.org/10.1130/G37165.1>, 2015.
- Tibbett, E. J., Scher, H. D., Warny, S., Tierney, J. E., Passchier, S., and Feakins, S. J.: Late Eocene Record of Hydrology and Temperature From Prydz Bay, East Antarctica, 36, e2020PA004204, <https://doi.org/10.1029/2020PA004204>, 2021.
- 620 Tierney, J. E. and Tingley, M. P.: A Bayesian, spatially-varying calibration model for the TEX₈₆ proxy, 127, 83–106, <https://doi.org/10.1016/j.gca.2013.11.026>, 2014.
- Tierney, J. E. and Tingley, M. P.: A TEX₈₆ surface sediment database and extended Bayesian calibration, 2, <https://doi.org/10.1038/sdata.2015.29>, 2015.



- 625 Tripathi, A. K., Eagle, R. A., Morton, A., Dowdeswell, J. A., Atkinson, K. L., Bahé, Y., Dawber, C. F., Khadun, E., Shaw, R. M. H., Shorttle, O., and Thanabalasundaram, L.: Evidence for glaciation in the Northern Hemisphere back to 44 Ma from ice-rafted debris in the Greenland Sea, 265, 112–122, <https://doi.org/10.1016/j.epsl.2007.09.045>, 2008.
- Uenzelmann-Neben, G. and Gruetzner, J.: Chronology of Greenland Scotland Ridge overflow: What do we really know?, *Marine Geology*, 406, 109–118, <https://doi.org/10.1016/j.margeo.2018.09.008>, 2018.
- 630 Vandenberghe, N., Hilgen, F. J., and Speijer, R. P.: The Paleogene Period, 855–921 pp., <https://doi.org/DOI:10.1016/B978-0-444-59425-9.00028-7>, 2012.
- Via, R. K. and Thomas, D. J.: Evolution of Atlantic thermohaline circulation: Early Oligocene onset of deep-water production in the North Atlantic, <https://doi.org/10.1130/G22545.1>, 2006.
- 635 Wade, B. S., Houben, A. J. P., Quaijtaal, W., Schouten, S., Rosenthal, Y., Miller, K. G., Katz, M. E., Wright, J. D., and Brinkhuis, H.: Multiproxy record of abrupt sea-surface cooling across the Eocene-Oligocene transition in the Gulf of Mexico, 40, 159–162, <https://doi.org/10.1130/G32577.1>, 2012.
- Weijers, J. W. H., Lim, K. L. H., Aquilina, A., Damsté, J. S. S., and Pancost, R. D.: Biogeochemical controls on glycerol dialkyl glycerol tetraether lipid distributions in sediments characterized by diffusive methane flux, <https://doi.org/10.1029/2011GC003724>, 2011.
- 640 Zachos, J. C., Quinn, T. M., and Salamy, K. A.: High-resolution (104 years) deep-sea foraminiferal stable isotope records of the Eocene-Oligocene climate transition, 11, 251–266, <https://doi.org/10.1029/96PA00571>, 1996.
- Zhang, Y. G., Zhang, C. L., Liu, X. L., Li, L., Hinrichs, K. U., and Noakes, J. E.: Methane Index: A tetraether archaeal lipid biomarker indicator for detecting the instability of marine gas hydrates, 307, 525–534, <https://doi.org/10.1016/j.epsl.2011.05.031>, 2011.
- 645 Zhang, Y. G., Pagani, M., Liu, Z., Bohaty, S. M., and DeConto, R.: A 40-million-year history of atmospheric CO₂, 371, 2013.
- Zhang, Y. G., Pagani, M., and Wang, Z.: Ring Index: A new strategy to evaluate the integrity of TEX86paleothermometry, 31, 220–232, <https://doi.org/10.1002/2015PA002848>, 2016.

650

655

660

665



670

Figure captions

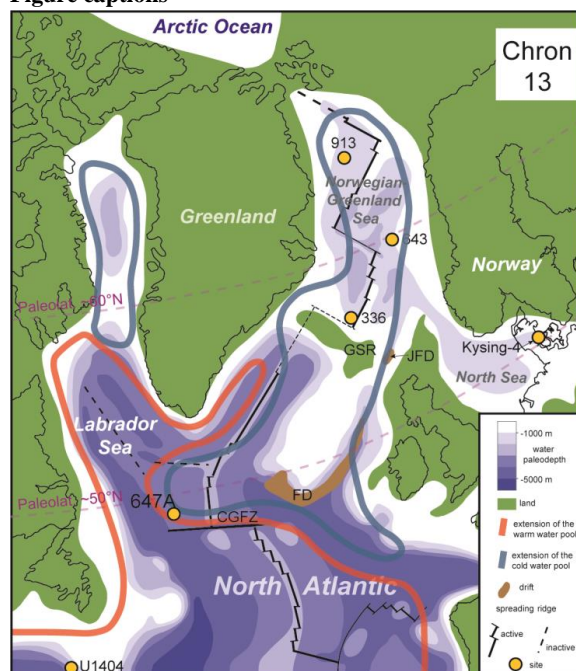


Figure 1: The late Eocene (magnetic polarity Chron 13; 33.705–33.157 Ma (GTS2012)) location of Site 647 (ODP Leg 105) and other sites studied for temperature proxies (pollen in ODP 913B, ODP 643, ODP 985 (Eldrett et al., 2009); alkenones in DSDP 336, ODP 913B and IODP U1404 (Liu et al., 2009, 2018); GDGTs in Kysing-4 (Śliwińska et al., 2019)) referred to in the text. The paleogeographic map is modified after Arthur et al., (1989), Piepjohn et al., (2016), Śliwińska et al., (2019) and references therein. Abbreviated oceanic features identified are: the Feni Drift (FD)(Davies et al., 2001), the Judd Falls Drift (JFD) (Hohbein et al., 2012), Greenland–Scotland Ridge (GSR), and Charlie-Gibbs Fracture Zone (CGFZ).

685

690

695

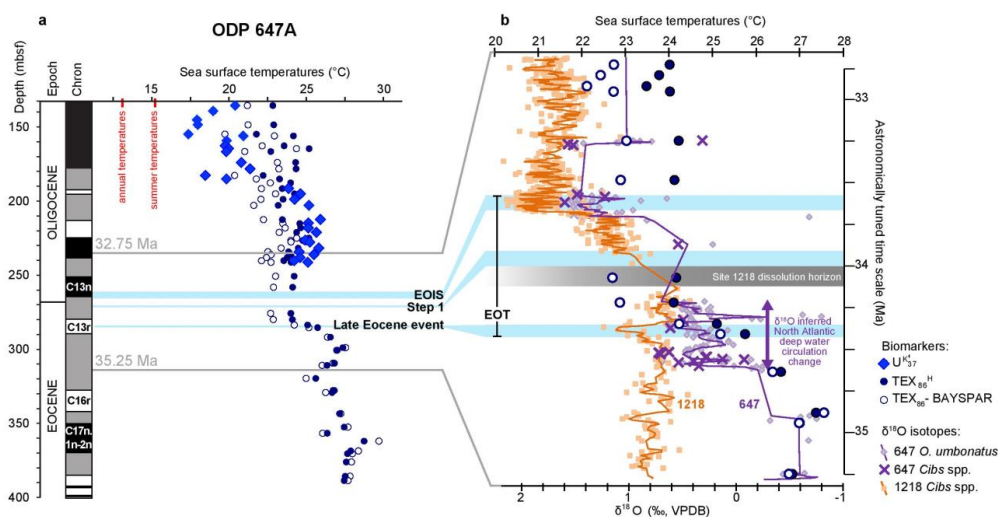
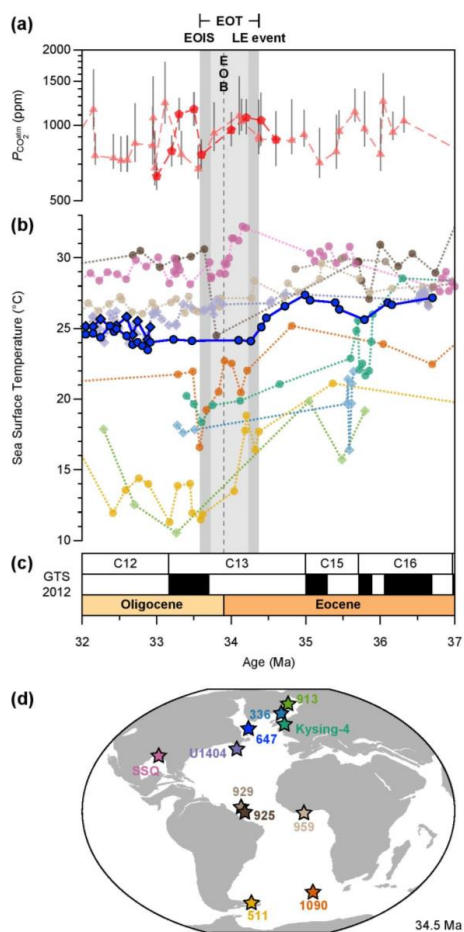


Figure 2: The sea surface temperature (SST) record from the Ocean Drilling Program (ODP) Site 647A. a) SSTs based on TEX_{86} and U^{K}_{37} indices (this study). Magnetostratigraphy after ref. (Firth et al., 2013). MAT – modern average annual temperatures (10.6 °C), ST – modern summer temperatures (15.2 °C) at the paleolocation of 46°N based on the Ocean World database. b) The new temperature record across the Eocene-Oligocene transition (EOT) compared to (i) benthic foraminifera oxygen stable isotope ($\delta^{18}\text{O}$) records from ODP Site 647 (*Oridorsalis umbonatus*; > 63 μm) (Coxall et al., 2018) and an inferred zone of acute North Atlantic deep water circulation change, and (ii) benthic $\delta^{18}\text{O}$ record from ODP Site 1218 providing the chemostratigraphic framework that allows us to extrapolate the EOIS, Step 1 and Late Eocene events to Site 647 (Coxall and Wilson, 2011). All ages are based on the GTS2012 (Vandenberghe et al., 2012).



710 **Figure 3:** SST evolution across the EOT in the Atlantic Ocean. a) Reconstructed $P_{CO_2^{atm}}$ based on planktonic
 foraminiferal $\delta^{11}B$ (pentagons) (Pearson et al., 2009) and phytoplankton alkenone $\delta^{13}C$ (triangles) (Pagani et al.,
 2011; Zhang et al., 2013). The effect of $P_{CO_2^{atm}}$ on radiative forcing scales logarithmically. b) Newly generated
 and published (Cramwinckel et al., 2018; Houben et al., 2019; Inglis et al., 2015; Liu et al., 2018, 2009;
 Śliwińska et al., 2019; Wade et al., 2012) reconstructed SSTs based on U_{37}^{kl} (diamonds) and TEX_{86}^H (circles). All
 715 ages are converted into the GTS2012 (Vandenberghe et al., 2012). c) Magneto- and chronostratigraphy based on
 the GTS2012 (Vandenberghe et al., 2012). d) Paleogeography at 34.5 Ma (<https://www.ods.de/>) with color-
 coded site locations of the SST records shown in panel B. SSQ stands for St. Stephen's Quarry.

720

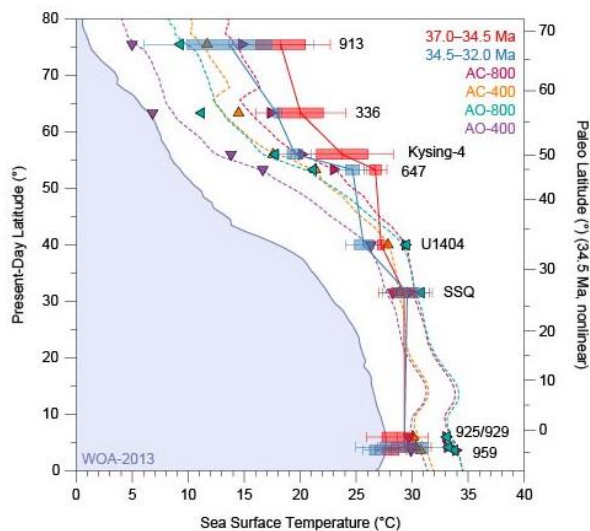
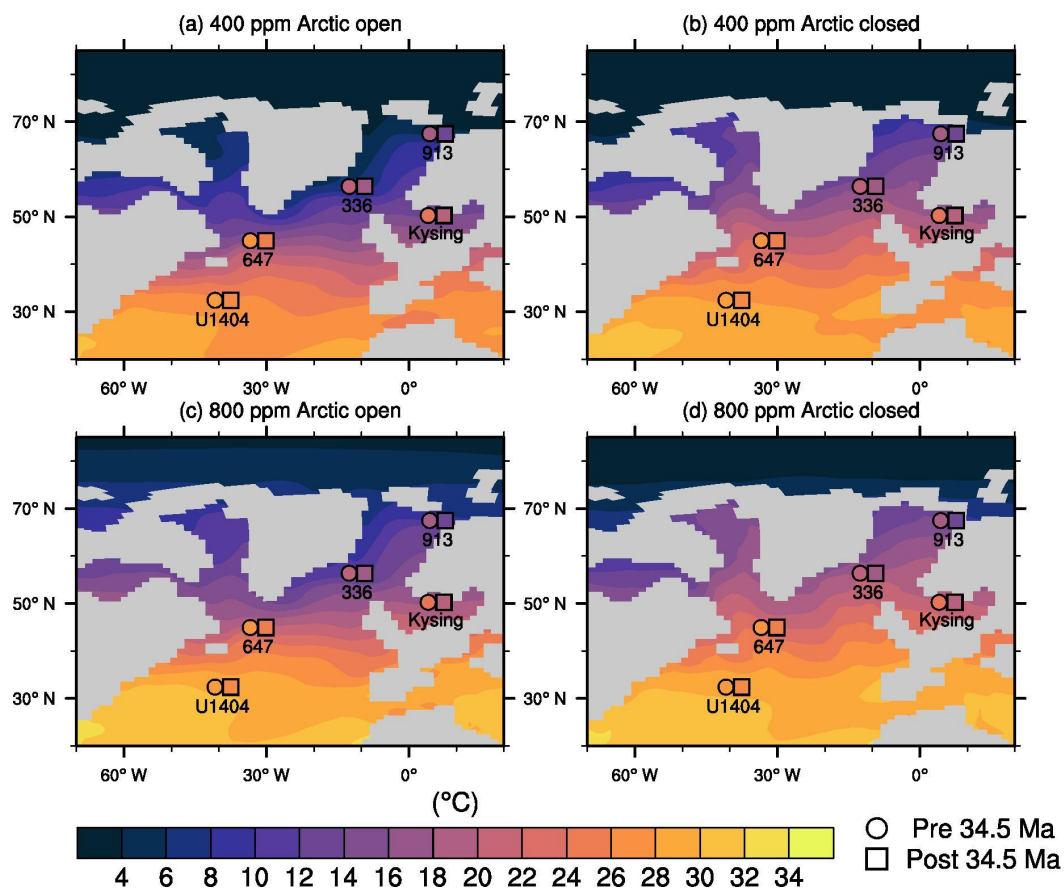


Figure 4: Data-model comparison of latitudinal SST gradients for the “Eocene” (>34.5 Ma, red bars and solid lines) and “Oligocene” (<34.5 Ma, blue bars and solid lines) states to the four different model simulations. The dashed lines show the zonal average SSTs at that latitude and the triangles show the site specific temperatures in the simulations. The 1 and 2 sigma error bars are indicated around the data points and on the left of the figure in solid blue is the zonally average present-day Atlantic SST from the World Ocean Atlas (Boyer et al., 2013). Model paleolatitudes (right hand axis) are shifted with respect to present-day latitudes of the data (site and WOA data, left hand axis) by the average offset of -7.0° (error: $\pm 1.5^\circ$) for the sites considered.

725

730

735



740

Figure 5: Comparison of model temperatures in the four simulations in the North Atlantic with Late Eocene (circles) and Early Oligocene (squares) proxy data. Contours show the modelled annual mean SST for the Arctic open (a, c) and the Arctic closed run (b, d) for atmospheric CO₂ concentrations of 400 ppm (a,b) and 800 ppm (c,d). The colored circles show the proxy data averaged between 34.5 and 37 Ma (a, b) and between 34.5 and 32 Ma (c, d).

745

750

755

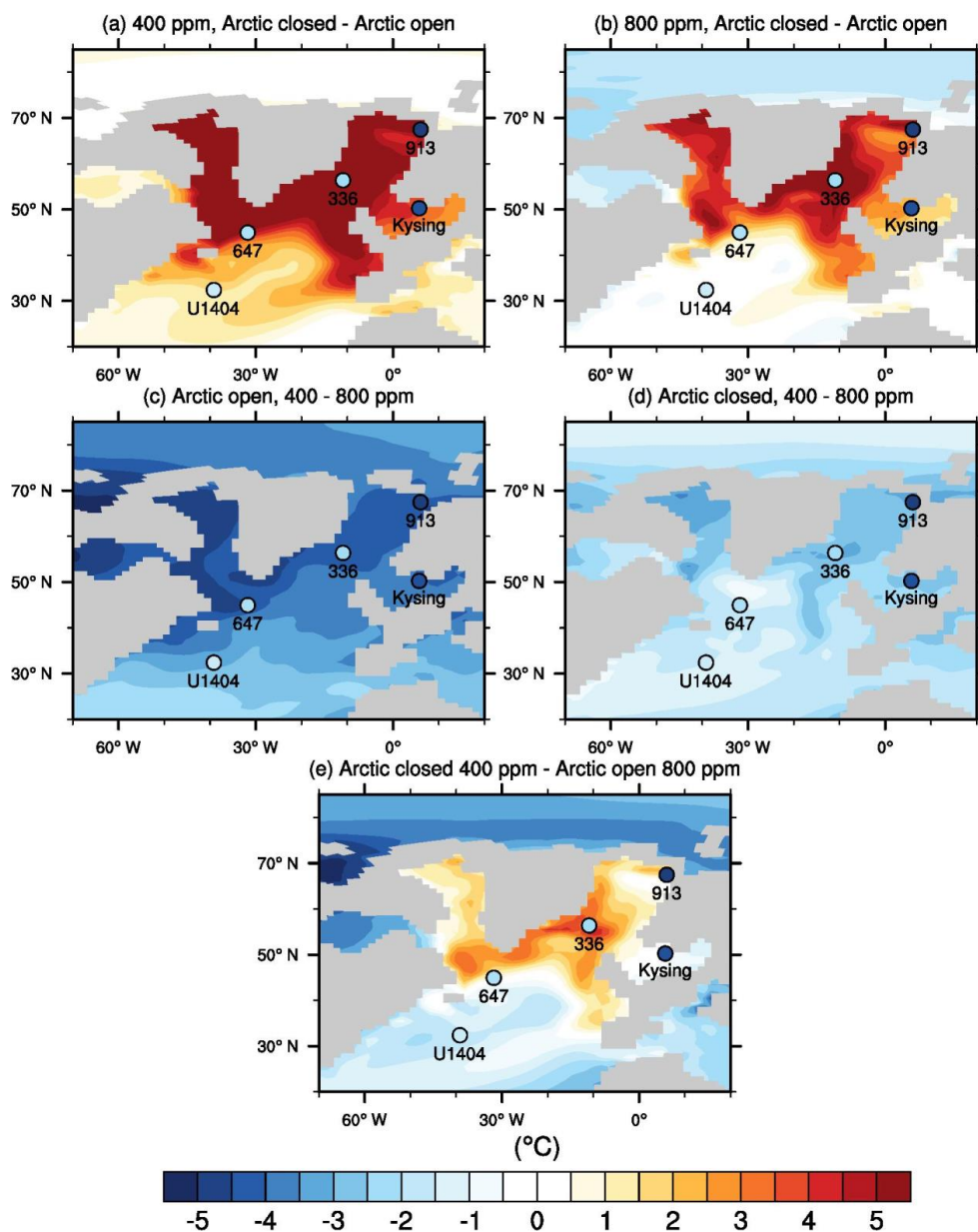
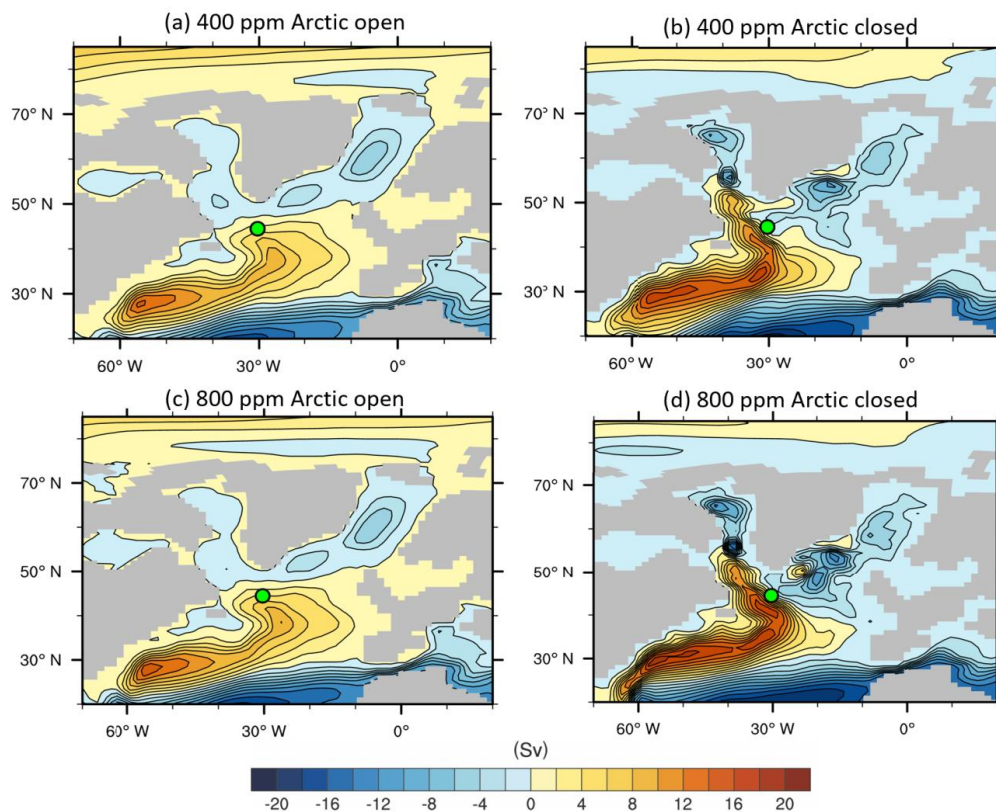


Figure 6: Site specific SST anomalies across the EOT from proxy data compared with SST differences between the model simulations. Shown is the SST impact of closing of the Arctic for a 400 ppm climate (a) and an 800 ppm climate (b) as well as the impact of reducing CO₂ from 800 ppm to 400 ppm when the Arctic is open (c) and when it is closed (d). The final subplot shows the difference between the 800 ppm open Arctic and the 400 ppm closed Arctic (e).

760



765 **Figure 7:** Barotropic streamfunctions illustrating the horizontal circulation (positive = clockwise) for the Arctic open (a, c) and the Arctic closed run (b, d) for atmospheric CO₂ concentrations of 400 ppm (a,b) and 800 ppm (c,d). The contour interval is 2 Sv.